DOI: 10.1002/ ((please add manuscript number))
Article type: Full Paper

Redox-Active Iron-Citrate Complex Regulated Robust Coating-Free Hydrogel Microfiber Net with High Environmental Tolerance and Sensitivity

Min Ju, Baohu Wu, Shengtong Sun and Peiyi Wu**

M. Ju, Prof. S. Sun, Prof. P. Wu
State Key Laboratory for Modification of Chemical Fibers and Polymer Materials, College of Chemistry, Chemical Engineering and Biotechnology, Center for Advanced Low-dimension Materials, Donghua University, Shanghai 201620, China.
E-mail: shengtongsun@dhu.edu.cn; wupeiyi@dhu.edu.cn
Dr. B. Wu
Jülich Centre for Neutron Science (JCNS) at Heinz Maier-Leibnitz Zentrum (MLZ)
Forschungszentrum Jülich, Lichtenbergstr. 1, 85748 Garching, Germany

Keywords: hydrogel microfiber; draw-spinning; iron-based redox chemistry; sensing; anti-freezing

Abstract: Stretchable hydrogel microfibers as a novel type of ionic conductors are promising in gaining skin-like sensing applications in more diverse scenarios. However, it remains a great challenge to fabricate coating-free but water-retaining conductive hydrogel microfibers with a good balance of spinnability and mechanical strength. Here we employed the old yet significant redox chemistry of Fe-citrate complex to solve this issue in the continuous draw-spinning process of poly(acrylamide-*co*-sodium acrylate) hydrogel microfibers and microfiber nets from its water/glycerol solution. The resultant microfibers are ionically conductive, highly stretchable and uniform with tunable diameters. Furthermore, the presence of redox-reversible Fe-citrate complex and glycerol endows the fibers with good anti-freezing, water-retaining and environmentally intelligent properties. Humidity and UV light can finely mediate the stiffness of hydrogel microfibers; conversely, the ionic conductance of microfibers is also responsive to light, humidity, and strain, which enables the highly sensitive perception of environmental changes. The present draw-spinning strategy provides more possibilities for coating-free conductive hydrogel microfibers with a variety of responsive and sensing applications.

1. Introduction

Stretchable hydrogel ionic conductors are appealing in recent skin-like sensing applications owing to their similarities to biological tissues and versatility in electrical and mechanical engineering.[1-2] Notably, current conductive hydrogel sensors are mainly based on the form of bulk films to perceive external stimuli via detectable electrical signal changes, which, to some content, hinders their applications in more diverse scenarios.[3-5] Moreover, due to the large size and isotropically uniform structure, the response and sensitivity of bulk hydrogels are also limited. Feasible methods to improve the sensory abilities of stretchable hydrogels are: i) introducing fugitive but recoverable conductive percolation networks,[6-8] or ii) minimizing hydrogels' sizes to increase effective sensing area;[9-10] wherein, miniatured hydrogel structures are of particular interest because of their high adaptability and customizability for meeting various sensing requirements.

One-dimensional conductive hydrogel microfibers could be the most important example of miniaturized hydrogels, whose fabrication are facing two main problems nevertheless:

1) dehydration vs. conductivity: severe dehydration easily occurs as the fiber is spun in air, although a few researches have highlighted the significance of dehydration for enhancing the fiber strength and stretchability.[11-13] There seems to be a trade-off for bare hydrogel microfibers between fiber strength and ionic conductivity, which depend on adverse water contents. To circumvent this issue, recently Ma et al reported a core-shell stretchable and conductive sodium polyacrylate hydrogel microfiber with a thin elastomer coating layer to prevent dehydration while maintaining good fiber elasticity.[14] Nonetheless, the inert elastomer coating evitably leads hydrogel microfiber to be insensitive to environmental changes, which are unfavorable for sensing applications.

2) spinnability vs. fiber strength: compared to electrospinning[15-16] and extrusion spinning,[9-10, 17-18] microfluidic or draw spinning inspired from spider spinning procedure[11-14, 19-20] seems to

be more suitable for fabricating long uniform hydrogel microfibers. However, unless using the strategy of full dehydration, it is still challenging to compromise the spinnability and mechanical strength of hydrogel microfibers. Gel spinning needs a flowable sol precursor while water as a strong plastizer would largely reduce the final fiber strength;[21] in other words, low or no crosslinking is essential for the spinning solution, yet high crosslinking is indispensable to compensate the water plasticizing effect.

In nature, by virtue of their abundance and redox properties, iron makes an ideal redox-active agent for many biologic or industrial processes.[22-24] For example, iron-based sensors including Fe-S clusters, heme, and mononuclear iron sites act as important switches to control protein activity in response to changes in cellular redox balance.[23] Iron gall ink, as a standard writing ink dating back to the Middle Ages in Europe, is made from water-soluble Fe(II) tannate complex, which converts to a dark water-insoluble Fe(III) tannate as exposed to air after writing on paper.[24] Moreover, the redox-active iron-citrate complex enables the reversible sol-gel transition in poly(acrylic acid) aqueous solution upon UV light illumination and air oxidation,[25] which was also recently employed for photo-detectable hydrogel adhesion.[26] Therefore, it is anticipated that iron-based redox chemistry could be an ideal solution for adjusting crosslinking densities in the spinning process of hydrogel microfibers.

On the basis of the above hypothesis, here we propose an iron-citrate redox chemistry-regulated draw spinning strategy for producing highly stretchable hydrogel microfibers and robust fiber nets with good water retention without elastomer coating. Glycerol was introduced which not only enhances the spinnability of spinning solution, but also improves the frost and dehydration resistance of coating-free hydrogel microfibers. Owing to all these merits, the resultant hydrogel fibers exhibit mechanical tunability via UV light and humidity, and the fiber's inherent ionic conductivity also enables highly sensitive sensations to various environmental stimuli, like force, UV light, and humidity.

2. Results and discussion

The spinning solution consists of long-chain poly(acrylamide-*co*-sodium acrylate) (P(AAm-*co*-AA), M_w ~ 520,000 g/mol), $FeCl_2$ and citric acid (CA) dissolved in a water/glycerol mixture. As shown in **Figure 1**a, hydrogel microfibers are directly drawn out of the spinning head and immediately solidify with the evaporation of excess water to reach a water-content equilibrium in air; collected by a rotating frame with controlled movement and collecting angles, the fibers can be woven into parallel arrays or nets (for fiber nets, the direction of rectangular rotating frame was tuned 90^o after finishing the collection of one-direction fiber arrays; see more details in the supporting information and Movie S1). The as-spun microfibers were left in air for ca. 7 days for natural oxidation to activate the high crosslinking of P(AAm-*co*-AA) chains by Fe^{3+}, following the above-mentioned redox-responsive transition of Fe-citrate complex.[25-26] The final hydrogel microfiber net is well aligned, uniform and elastic, and can sustain a certain weight of load like a fishing net (Figure 1b). In principle, any woven 2D or 3D organized patterns with tunable fiber densities can be obtained with this method.[19, 27] As an example, three fiber nets with different fiber densities were obtained by changing the parallel movement speed of rotating collector (Figure S1, Supporting Information).

We emphasize that it is crucial to choose the reversible redox-responsive Fe-citrate complex for draw spinning to compromise fiber spinnability and fiber strength: strong crosslinking from trivalent ions (Fe^{3+} or Al^{3+}) leads to strong hydrogels with no spinnability (Figure S2, Supporting Information), while weak crosslinking from divalent ions (Zn^{2+}, Co^{2+}, Mg^{2+}, Ca^{2+}, Sr^{2+}) favors spinnability but the spun hydrogel fibers are mechanically too weak (Movie S2, Supporting Information). The strongest crosslinking of Fe(III)-PAA is evidenced from a lowest wavenumber of $\nu(COO^-)$ at 1550 cm^{-1} compared to all the studied divalent cations (Figure S3, Supporting Information), and such a strong complex was often used to design tough hydrogels.[28-29] By delicately

optimizing the spinning solution compositions in view of rheological plasticity, proper oxidation time, fiber strength and elongation (Table S1, Figure S4~S11, Supporting Information), the solvent of 1:1 glycerol/water (weight ratio), polymer concentration of 30 wt%, and the molar ratio, [AA]:[$FeCl_2$]:[CA] = 3:1:1, were found to be most suitable for draw-spinning hydrogel microfibers.

The dried P(AAm-*co*-AA)/Fe(III) hydrogel microfiber shows a cylindrical shape, and the fractured surface reveals a compact and homogenous interior core (Figure 1c). Synchrotron FTIR micro-spectroscopy was used to further confirm the structural uniformity of hydrogel microfibers, which exhibit the even spectral intensity distribution of $\nu(CH_2)$ (2937 cm^{-1}), amide II (1613 cm^{-1}) and ν(C-O) (1045 cm^{-1}), as well as the almost identical whole spectra at different positions along the fiber (Figure S12, Supporting Information). As suggested in Figure 1d and e, the diameter of hydrogel microfiber can be finely adjusted from 30 to 120 μm by changing the syringe feeding speed and collector rotational speed. Unless otherwise stated in this paper, the feeding and rotational speeds were fixed to 100 μL/min and 7.5 rpm respectively, leading to a fiber diameter of 85 ± 10 μm. Moreover, the draw-spinning process also produces very good preferential chain orientation of hydrogel fibers, as indicated by the asymmetrical 2D SAXS pattern perpendicular to fiber axis and a sharp Azimuth plot (FWHM ~ 6.5º) (Figure 1f). SAXS result suggests that the inter-distance of fibrillar nanostructure in the fiber is ~33 nm (Figure S13, Supporting Information).

The hydrogel microfibers are highly elastic with good stretchability and cyclability. The fiber can be stretched five times the original length with an elastic modulus of 0.27 MPa, and the cycling curves at different strains (50% - 250%) coincides well with the single tensile curve to break (**Figure 2**a). Apparent hysteresis loops are observed on the loading–unloading curves, indicating that hydrogel microfibers could dissipate energy effectively through the dynamic and recoverable coordination between Fe(III) and the

carboxylate groups of polymer chains.[28] Such supramolecular crosslinking nature is further supported by the increased elastic moduli when stretching at higher speeds (Figure S14, Supporting Information).[30-31] It is also noted that the elastic modulus of P(AAm-*co*-AA)/Fe(III) hydrogel microfiber is smaller than that of previously reported Fe(III)-crosslinked P(AAm-*co*-AA) bulk hydrogel (~0.5-3.5 MPa),[28] probably due to the presence of glycerol which weakens the coordination between carboxylate groups of polymer and Fe(III) (Figure S15, Supporting Information). Cyclic loading-unloading tests were also carried out with different waiting time at a fixed strain of 200% (Figure 2b). A residual strain of 18% was observed for the first unloading, which can be totally eliminated by waiting 20 min, indicating the complete self-recovery of viscoelastic deformation. The high elasticity of hydrogel microfibers was also supported by the in-situ imaging of needle-based three-point bending test (Figure S16, Supporting Information).

In contrary to conventional hydrogel microfibers that would freeze and lose elasticity at subzero temperatures, P(AAm-*co*-AA)/Fe(III) hydrogel microfibers exhibit excellent anti-freezing behavior. As shown in DSC curve (Figure 2c), a freezing point of -61 ^{o}C was detected for the hydrogel fiber at RH = 90%. Tensile stress-strain curves of hydrogel microfibers were collected by controlling the environmental temperature (Figure 2d). It is observed that the hydrogel microfiber maintains good elasticity at -40 ^{o}C with almost coincident tensile curve to that at 25 ^{o}C, and the fiber becomes brittle lower than -50 ^{o}C. The frost resistance of hydrogel microfiber is attributed to the presence of glycerol, which is known to significantly inhibit ice crystallization in hydrogel systems.[32-33]

Due to the large surface area and excellent hygroscopicity of glycerol, the hydrogel microfiber is water-retaining at ambient conditions without any coating protection. As calculated by TGA (Figure S17, Supporting Information), with increasing the humidity

from 30% to 90%, the equilibrium water content increases from 5.7 wt% to 28.5 wt%, while the glycerol content remains unchanged relative to the mass of polymer (**Figure 3**a). Such water-content sensitivity features the tunability of hydrogel microfiber stiffness by humidity. As expected, the tensile stress-strain curves of hydrogel microfibers show a remarkable reduction of both the moduli and fracture stresses with increasing humidity (Figure 3b). Nevertheless, at constant humidity, the water and glycerol contents are basically unchanged, suggesting the good stability of hydrogel microfiber for long-term storage (Figure S18, Supporting Information).

As mentioned above, the redox reaction between Fe(II)- and Fe(III)-citrate complexes in the hydrogel microfiber is reversible upon natural oxidation and UV light reduction. The frequency of $\nu(COO^-)$ is an ideal indicator to monitor the redox reaction, as $\nu(COO^-)$ is largely influenced by the valence states of iron ions (for Fe^{2+}, 1558 cm^{-1}; for Fe^{3+}, 1550 cm^{-1}; Figure S19, Supporting Information). With oxidation, $\nu(C=O)$ shifted gradually from 1558 cm^{-1} to 1550 cm^{-1} and reached a plateau after 7 days (Figure 3c). Conversely, the photoreduction process is fully reversible and pretty fast with a plateau being reached within 120 s (Figure 3d). This redox cycle be repeated for about four times until the complete consumption of CA in the photoreduction process[25] (Figure S20, Supporting Information). It is expectable that the reduction of Fe(III) to Fe(II) would inevitably lead to the mechanical weakening of hydrogel microfibers. Upon UV illumination for 60 s and 120 s, the fracture stress and strain of hydrogel microfibers are significantly reduced (Figure 3e). The effect of UV light intensity on the mechanical stiffness of hydrogel microfibers is evidenced by the stress relaxation measurements. At a fixed tensile strain of 100%, the hydrogel microfibers produced faster relaxation with higher UV light intensities (Figure 3f). All these findings reveal that the stiffness of P(AAm-*co*-PAA)/Fe(III) hydrogel microfibers is easily tunable with adjusting humidity and UV light irradiation time or intensity.

Similar to many other ion-containing hydrogels,[5, 7, 34] P(AAm-*co*-PAA)/Fe(III) hydrogel microfibers are ionically conductive due to good water-retention and the presence of mobile ions like Na^+, Cl^-, and Fe^{2+}/Fe^{3+}. The conductivity of hydrogel microfiber is calculated to be about 4.2 mS/m at the relative humidity of 60%, which can be further improved with the addition of more salts like NaCl (Figure S21, Supporting Information). Therefore, the unique UV light and humidity responsiveness could bring resistive sensing properties. As shown in **Figure 4**a, a hydrogel microfiber net fixed on a glass plate was placed in a dark box and exposed to UV light while the multimeter was used to monitor the resistance variations $\Delta R/R_0 = (R-R_0)/R_0$, where R_0 and R represent the initial and real-time resistances, respectively. To distinguish the influence of photothermal effect on UV light response, P(AAm-*co*-AA)/Fe(III) hydrogel films with and without CA were first tested (no photoreduction occurs without CA[35]). As both films were irradiated by UV light (365 nm, 81 mW/cm^2), the resistance of the film containing CA decreased apparently faster than that without CA (Figure 4b), suggesting that UV light is suitable as a stimulus to induce resistance changes. The absolute $\Delta R/R_0$ value of hydrogel microfiber net increases monotonically with increasing UV light intensity (Figure 4c), which is understandable because UV irradiation reduces the polymer crosslinking density and thus increases the ion migration rate or conductivity of hydrogel microfiber. Figure 4d shows the resistance changes of hydrogel microfiber net generated by intermittent UV irradiation with variable light intensities (much weaker changes for hydrogel without CA, Figure S22, Supporting Information), indicating that the hydrogel microfiber can be applied to perceive UV irradiation with different light intensities.

Similarly, humidity can also be sensed from the resistance changes of hydrogel microfiber net. Switching the humidity from 90% to 11%, 30%, or 60% causes a significant resistance increase, as a lower water content would remarkably slow down

ion migration rate (Figure 4e, experimental setup in Figure S23, Supporting Information). Furthermore, the hydrogel microfibers can also serve as a strain sensor. As hydrogel microfiber is stretched, the resistance increases nonlinearly upward with strain (Figure 4f), and the relationship can be mathematically described as, $\Delta R/R_0 = \varepsilon^2 + 2\varepsilon$ (ε, strain; see calculation details in Supporting Information). The resistance increases monotonically with applying a strain of 25%, 50%, 100% and subsequently returning to the initial value, verifying the good signal repeatability of hydrogel microfiber as a resistive sensor upon cyclic loading. To further demonstrate the resistive sensing ability of hydrogel microfiber, we repeatably dropped a table tennis ball on the fiber net and then picked it up after a certain period. Because the microfiber net is elastic, the tennis ball would oscillate before a stationary state was reached. It is interesting to find that the real-time resistance changes of hydrogel microfiber net can fully monitor the whole process with good repeatability (Figure 4g).

3. Conclusion

In terms of the trade-offs of hydrogel microfibers between dehydration and conductivity as well as between spinnability and fiber strength, we report in this paper a novel strategy on the basis of redox-active Fe-citrate complex regulation for continuous draw-spinning robust and conductive P(AAm-*co*-AA) hydrogel microfibers from a water/glycerol solution. The spinning method is able to easily adjust fiber diameters and produce well-arranged fiber nets, and subsequent natural oxidation converting Fe(II) to Fe(III) with higher crosslinking generates anti-freezing and water-retaining hydrogel microfibers with high tensile strength and about five times elongation. Moreover, the fiber stiffness can be easily adjusted by UV light and humidity, which also makes hydrogel microfiber resistively ‘smart’ to various environmental stimuli. We anticipate that the reported

redox-chemistry guided draw-spinning method can be potentially extended to prepare other intelligent hydrogel fibers with more advanced sensing and actuating applications.

Supporting Information
Supporting Information is available from the Wiley Online Library or from the author.

Acknowledgements

We gratefully acknowledge the financial support from the National Science Foundation of China (NSFC) (Nos. 21991123, 51873035, 51733003, 21604024), Shanghai Municipal Natural Science Foundation (17ZR1440400), "Qimingxing Plan" (19QA1400200), "Chenguang Program" supported by Shanghai Education Development Foundation and Shanghai Municipal Education Commission (16CG32), and the Fundamental Research Funds for the Central Universities. We also thank the staffs from BL01B and BL16B beamlines at Shanghai Synchrotron Radiation Facility, for assistance during data collection.

Received: ((will be filled in by the editorial staff))
Revised: ((will be filled in by the editorial staff))
Published online: ((will be filled in by the editorial staff))

References

[1] C. Yang, Z. Suo, *Nat. Rev. Mater*. **2018**, *3*, 125-142.

[2] H. Yuk, B. Lu, X. Zhao, *Chem. Soc. Rev.* **2019**, *48*, 1642-1667.

[3] J. Y. Sun, C. Keplinger, G. M. Whitesides, Z. Suo, *Adv. Mater.* **2014**, *26*, 7608-7614.

[4] C.-C. Kim, H.-H. Lee, K. H. Oh, J.-Y. Sun, *Science* **2016**, *353*, 682-687.

[5] Z. Lei, P. Wu, *Nat. Commun.* **2018**, *9*, 1134.

[6] L. Pan, A. Chortos, G. Yu, Y. Wang, S. Isaacson, R. Allen, Y. Shi, R. Dauskardt, Z. Bao, *Nat. Commun.* **2014**, *5*, 3002.

[7] Z. Lei, Q. Wang, S. Sun, W. Zhu, P. Wu, *Adv. Mater.* **2017**, *29*, 1700321.

[8] Y.-Z. Zhang, K. H. Lee, D. H. Anjum, R. Sougrat, Q. Jiang, H. Kim, H. N. Alshareef, *Sci. Adv.* **2018**, *4*, eaat0098.

[9] Z. Lei, Q. Wang, P. Wu, *Mater. Horiz.* **2017**, *4*, 694-700.

[10] K. Tian, J. Bae, S. E. Bakarich, C. Yang, R. D. Gately, G. M. Spinks, M. in het Panhuis, Z. Suo, J. J. Vlassak, *Adv. Mater.* **2017**, *29*, 1604827.

[11] Y. Wu, D. U. Shah, C. Liu, Z. Yu, J. Liu, X. Ren, M. J. Rowland, C. Abell, M. H. Ramage, O. A. Scherman, *Proc. Natl. Acad. Sci. U.S.A.* **2017**, *114*, 8163-8168.

[12] Y. Wu, D. U. Shah, B. Wang, J. Liu, X. Ren, M. H. Ramage, O. A. Scherman, *Adv. Mater.* **2018**, *30*, 1707169.

[13] Y. Dou, Z. P. Wang, W. He, T. Jia, Z. Liu, P. Sun, K. Wen, E. Gao, X. Zhou, X. Hu, J. Li, S. Fang, D. Qian, Z. Liu, *Nat. Commun.* **2019**, *10*, 5293.

[14] X. Zhao, F. Chen, Y. Li, H. Lu, N. Zhang, M. Ma, *Nat. Commun.* **2018**, *9*, 3579.

[15] S. Jiang, F. Liu, A. Lerch, L. Ionov, S. Agarwal, *Adv. Mater.* **2015**, *27*, 4865-4870.

[16] L. Liu, S. Jiang, Y. Sun, S. Agarwal, *Adv. Funct. Mater.* **2016**, *26*, 1021-1027.

[17] A. L. Rutz, K. E. Hyland, A. E. Jakus, W. R. Burghardt, R. N. Shah, *Adv. Mater.* **2015**, *27*, 1607-1614.

[18] X. Liu, H. Yuk, S. Lin, G. A. Parada, T.-C. Tang, E. Tham, C. de la Fuente-Nunez, T. K. Lu, X. Zhao, *Adv. Mater.* **2018**, *30*, 1870021.

[19] Q. Li, Z. Xu, X. Du, X. Du, H. Cheng, G. Wu, C.-F. Wang, Z. Cui, S. Chen, *Chem. Mater.* **2018**, *30*, 8822-8828.

[20] P. Wei, K. Hou, T. Chen, G. Chen, I. T. Mugaanire, M. Zhu, *Mater. Horiz.* **2020**, DOI: 10.1039/c9mh01390c.

[21] J. Wang, S. Sun, B. Wu, L. Hou, P. Ding, X. Guo, M. A. Cohen Stuart, J. Wang, *Macromolecules* **2019**, *52*, 8643-8650.

[22] M. J. Sever, J. T. Weisser, J. Monahan, S. Srinivasan, J. J. Wilker, *Angew. Chem. Int. Ed.* **2004**, *43*, 448-450.

[23] F. W. Outten, E. C. Theil, *Antioxid. Redox Signaling* **2009**, *11*, 1029-1046.

[24] H. Lee, W. I. Kim, W. Youn, T. Park, S. Lee, T. S. Kim, J. F. Mano, I. S. Choi, *Adv. Mater.* **2018**, *30*, e1805091.

[25] F. Peng, G. Li, X. Liu, S. Wu, Z. Tong, *J. Am. Chem. Soc.* **2008**, *130*, 16166-16167.

[26] Y. Gao, K. Wu, Z. Suo, *Adv. Mater.* **2019**, *31*, 1806948.

[27] L. L. Xu, C. F. Wang, S. Chen, *Angew. Chem. Int. Ed.* **2014**, *53*, 3988-3992.

[28] P. Lin, S. Ma, X. Wang, F. Zhou, *Adv. Mater.* **2015**, *27*, 2054-2059.

[29] S. Y. Zheng, H. Ding, J. Qian, J. Yin, Z. L. Wu, Y. Song, Q. Zheng, *Macromolecules* **2016**, *49*, 9637-9646.

[30] C. H. Li, C. Wang, C. Keplinger, J. L. Zuo, L. Jin, Y. Sun, P. Zheng, Y. Cao, F. Lissel, C. Linder, X. Z. You, Z. Bao, *Nat. Chem.* **2016**, *8*, 618-624.

[31] Y. Cao, T. G. Morrissey, E. Acome, S. I. Allec, B. M. Wong, C. Keplinger, C. Wang, *Adv. Mater.* **2017**, *29*, 1605099.

[32] F. Chen, D. Zhou, J. Wang, T. Li, X. Zhou, T. Gan, S. Handschuh‐Wang, X. Zhou, *Angew. Chem. Int. Ed.* **2018**, *57*, 6568-6571.

[33] X.-F. Zhang, X. Ma, T. Hou, K. Guo, J. Yin, Z. Wang, L. Shu, M. He, J. Yao, *Angew. Chem. Int. Ed.* **2019**, *58*, 7366-7370.

[34] Z. Lei, P. Wu, *ACS Nano* **2018**, *12*, 12860-12868.

[35] C. Zhang, L. Wang, F. Wu, N. Deng, *Environ. Sci. Pollut. R.* **2006**, *13*, 156-160.

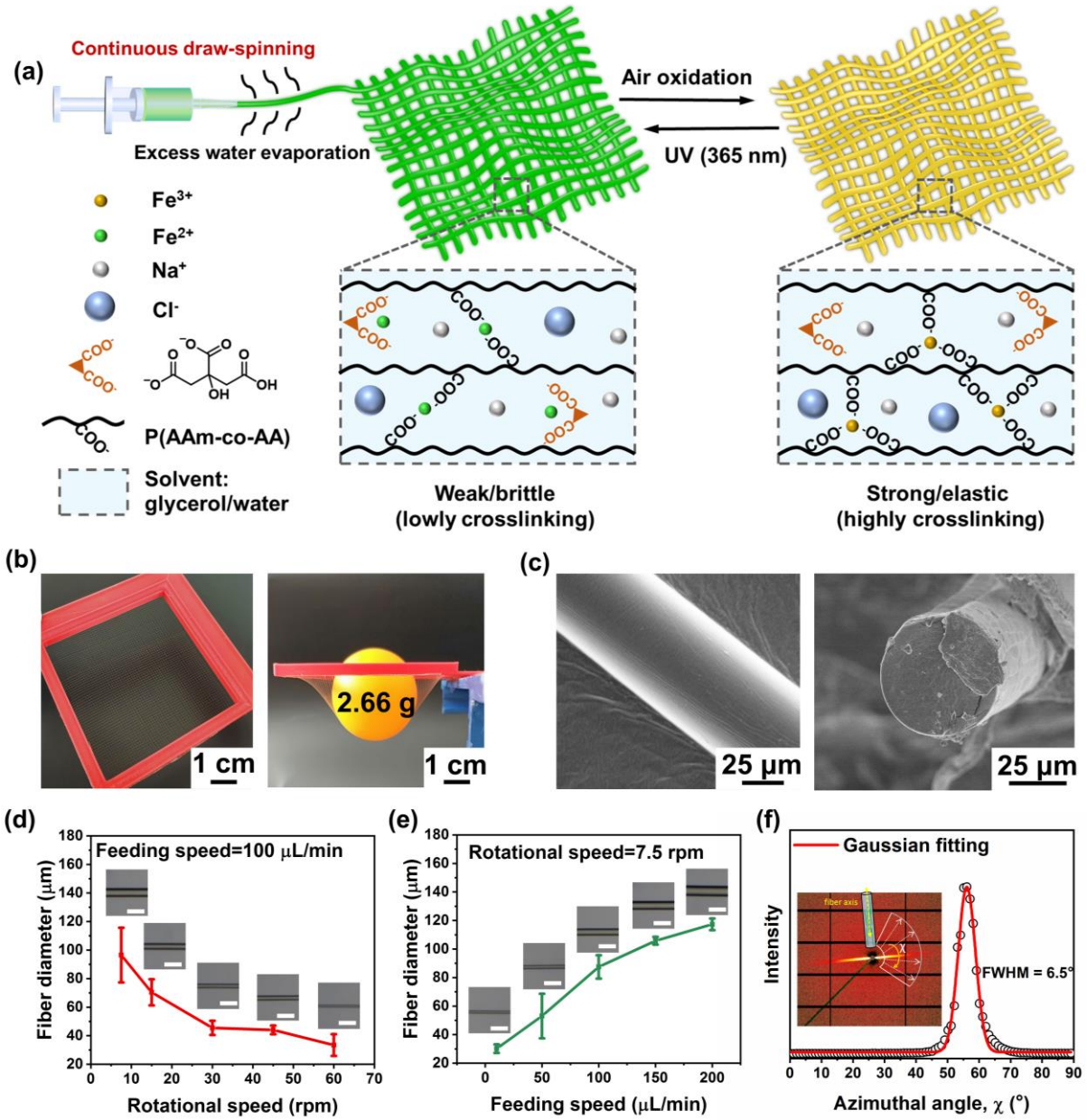

Figure 1. (a) Schematic fabrication of robust and conductive P(AAm-*co*-PAA)/Fe(III) hydrogel microfiber net via draw-spinning from a spinning dope of P(AAm-*co*-PAA) (sodium salt), $FeCl_2$, and citric acid dissolved in glycerol/water mixture followed by natural oxidation in air. The reversible redox-responsive Fe-citrate complex compromises fiber spinnability and strength, and endows UV light-mediated stiffness and sensing of hydrogel microfibers. (b) The spun hydrogel microfiber net is well aligned, elastic and can withstand a table tennis ball (~2.66 g). (c) SEM images of the external and fractured surfaces of dried hydrogel microfiber. (d, e) Fiber diameters as a function of rotational and feeding speeds. The insets show the optical images of as-spun hydrogel microfibers (scale bar, 200 μm). (f) 2D SAXS scattering pattern and the Azimuth integration plot of single hydrogel microfiber (inset is corresponding 2D image).

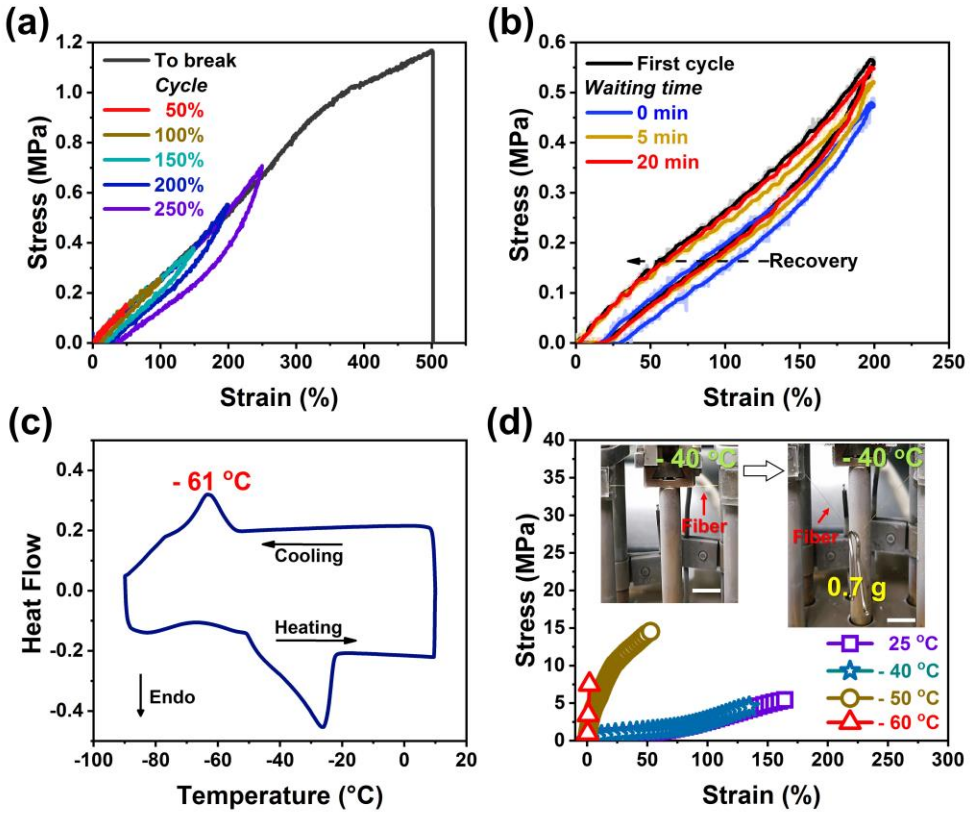

Figure 2. (a) Tensile stress-strain curves of P(AAm-*co*-PAA)/Fe(III) hydrogel microfibers and hysteresis loops measured at different strains (stretching rate: 10 mm/min). (b) Cyclic loading-unloading curves with different waiting time at a fixed strain of 200%. (c) DSC heating and cooling curve of hydrogel microfibers incubated at RH = 90%. (d) Tensile curves of hydrogel microfiber at different temperatures. The inset pictures show that the microfiber remains elastic at -40 ^{o}C as stretched by a weight of 0.7 g.

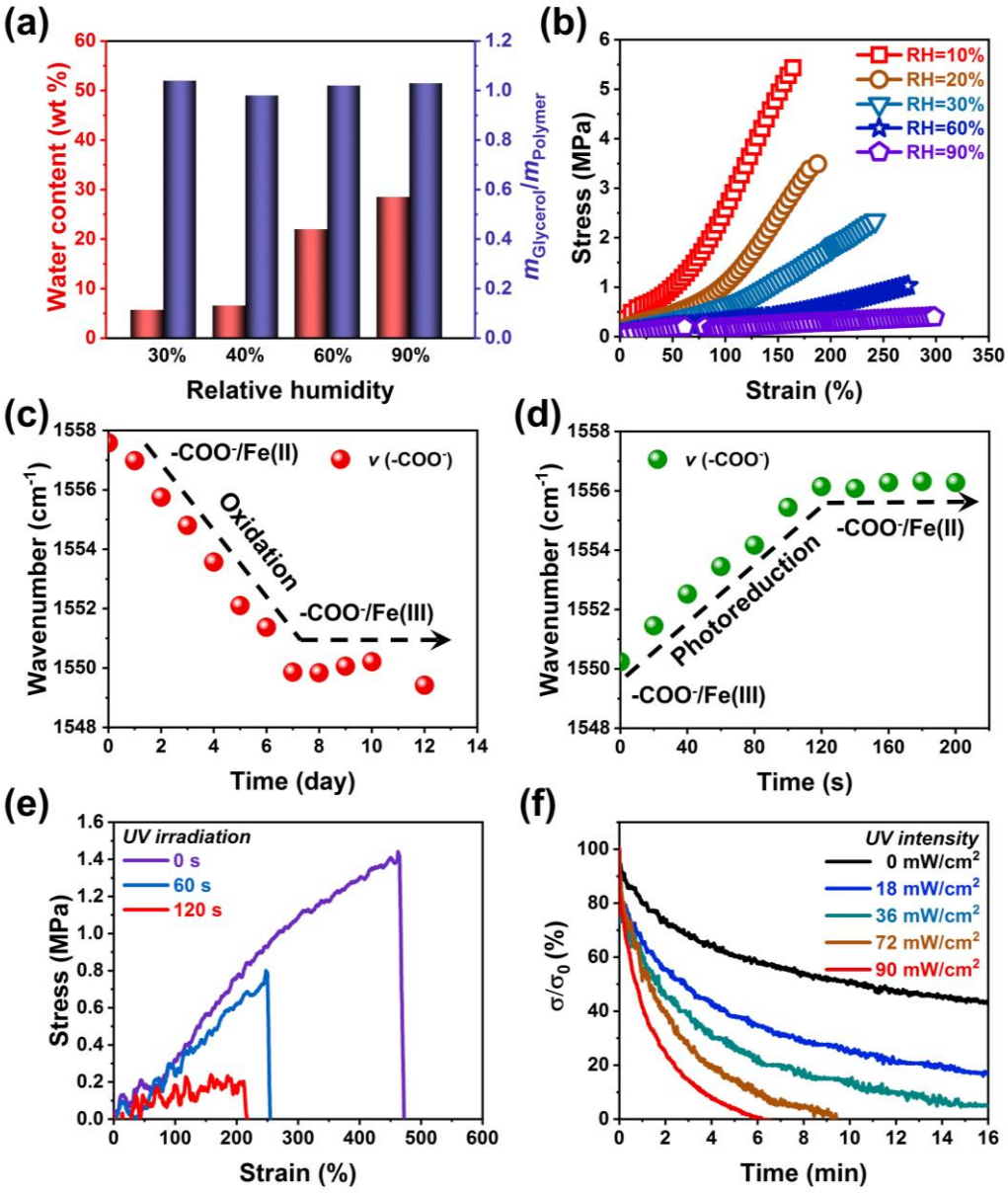

Figure 3. (a) Water and glycerol contents and (b) tensile curves of P(AAm-*co*-PAA)/Fe(III) hydrogel microfibers at different relative humidities. (c, d) Time-resolved wavenumber shifts of $\nu(COO^-)$ in the processes of natural oxidation and photoreduction (365 nm, 72 mW/cm^2), respectively. (e) Tensile curves of hydrogel microfiber upon UV irradiation (72 mW/cm^2) for 0 s, 60 s, and 120 s. (f) Stress relaxation curves of hydrogel microfibers under different intensities of UV irradiation with a fixed tensile strain of 100%.

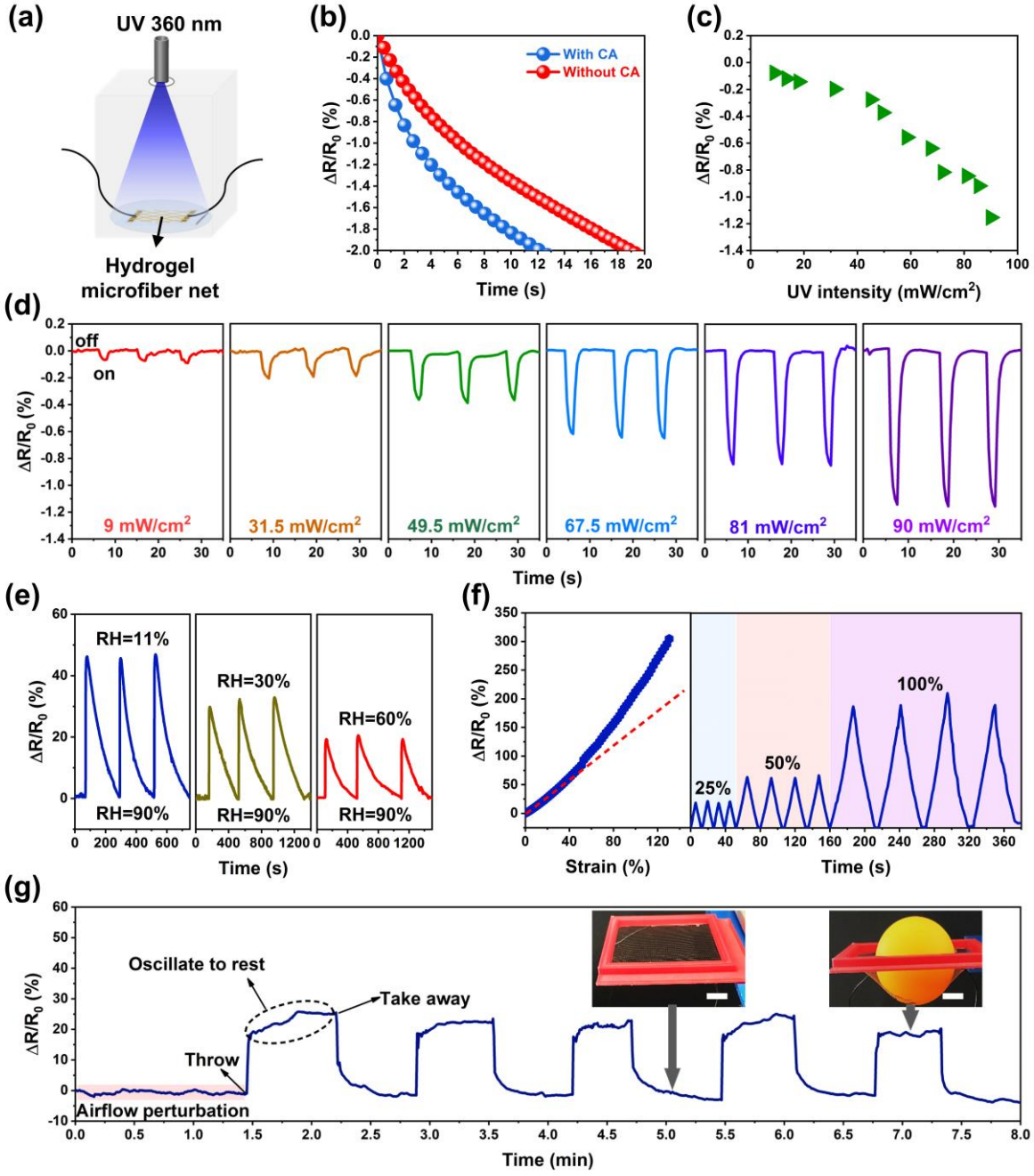

Figure 4. (a) Schematic illustration of the UV light sensing of hydrogel microfiber net. (b) Resistance changes of P(AAm-*co*-AA)/Fe(III) hydrogel films with and without CA as a function of UV light duration. (c) UV light intensity-dependent resistance changes and (d) real-time response curves of hydrogel microfiber net generated by intermittent UV light irradiation (~2 s pulse). (e) Resistance changing curves as humidity switches between RH 90% and 11%, 30%, or 60%. (f) Tensile strain-dependent resistance changes and real-time response curves measured at a maximum strain of 25%, 50%, and 100% for four cycles. (g) Real-time monitoring resistance changes of a hydrogel microfiber net by throwing and picking up a table tennis ball on it for five times. Scale bar, 1 cm.

Table of contents entry

Keyword: hydrogel microfiber, draw-spinning, iron-based redox chemistry, sensing, anti-freezing

Min Ju, Baohu Wu, Shengtong Sun* and Peiyi Wu*

Redox-Active Iron-Citrate Complex Regulated Robust Coating-Free Hydrogel Microfiber Net with High Environmental Tolerance and Sensitivity

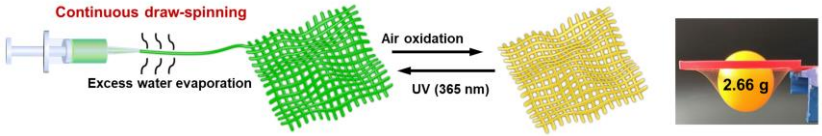

The iron-citrate complex-based redox chemistry allows for continuous draw-spinning of highly stretchable, uniform, and conductive hydrogel microfiber nets with excellent freezing and dehydration resistance, tunable mechanical stiffness, and electrical sensitivity to a variety of environmental changes.